Supporting Information

Characterizing the Heterogeneity of Small Extracellular Vesicle Populations in Multiple Cancer Types via an Ultrasensitive Chip

Jing Wang[1,10], Alain Wuethrich[1,], Richard J. Lobb[1], Fiach Antaw[1], Abu Ali Ibn Sina[1], Rebecca E. Lane[1], Quan Zhou[2], Chloe Zieschank[2], Caroline Bell[3], Vanessa F Bonazzi[4], Lauren G Aoude[4], Sarah Everitt[5,6], Belinda Yeo[3,7], Andrew P Barbour[4,8], Andreas Möller[9], and Matt Trau[1,2,*]*

[1]Centre for Personalized Nanomedicine, Australian Institute for Bioengineering and Nanotechnology (AIBN), The University of Queensland, Brisbane, QLD 4072, Australia

[2]School of Chemistry and Molecular Biosciences, The University of Queensland, Brisbane, QLD 4072, Australia

[3]Olivia Newton-John Cancer Research Institute and La Trobe University School of Cancer Medicine, 145 Studley Road, Heidelberg, VIC 3084, Australia

[4]The University of Queensland Diamantina Institute, The University of Queensland, Brisbane, QLD 4102, Australia

[5]Department of Radiation Therapy, Peter MacCallum Cancer Centre, Melbourne, VIC 3000, Australia.

[6]Sir Peter MacCallum Department of Oncology, Faculty of Medicine, Dentistry and Health Sciences, University of Melbourne, Parkville, VIC 3052, Australia

[7]Austin Health, Heidelberg, VIC 3084, Australia

[8]Queensland Melanoma Project, Princess Alexandra Hospital, Brisbane, QLD 4102, Australia

[9]Tumour Microenvironment Laboratory, QIMR Berghofer Medical Research Institute, Herston, QLD 4006, Australia

[10]Current address: Key Laboratory of OptoElectronic Science and Technology for Medicine, Ministry of Education, Fujian Provincial Key Laboratory for Photonics Technology, Fujian Normal University, Fuzhou 350007, China.

*Corresponding authors: a.wuethrich@uq.edu.au and m.trau@uq.edu.au

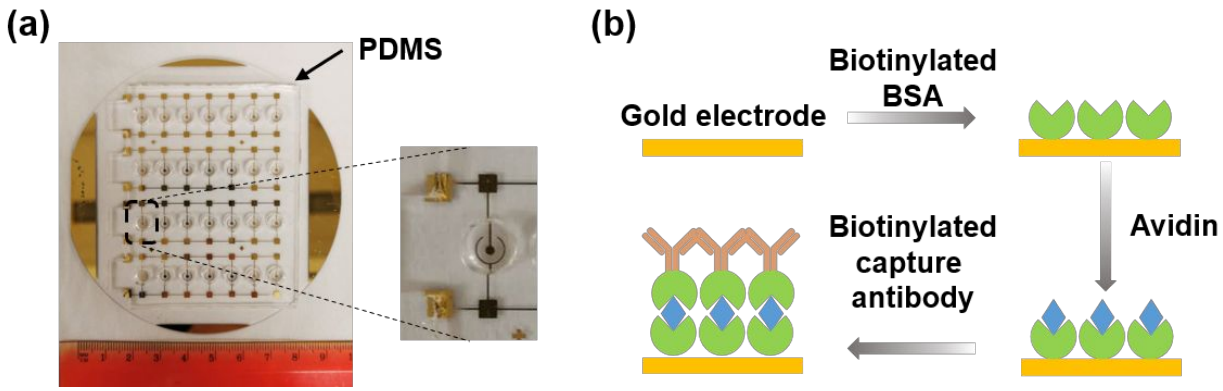

Fig. S1. ESCP design and functionalization. (a) A digital image of ESCP. Briefly, ESCP is made from a glass substrate with 7 × 4 array of sensing units and a covering polydimethylsiloxane (PDMS) layer carrying the microfluidic wells. Each sensing unit is made up of asymmetric inner circular (diameter = 1000 µm) and outer ring (width = 120 µm) structured gold electrodes that are spaced apart 1000 µm and connected to individual gold connecting pads that form the cathode and anode. (b) ESCP functionalization. The ESCP device covered with a PDMS slab is sequentially incubated with biotinylated bovine serum albumin (BSA) for 2 h, avidin for 1 h, biotinylated capture antibodies for 2 h at room temperature. The wells are washed with PBS buffer to remove excess reagents after each incubation step and blocked with BSA after functionalization with capture antibodies.

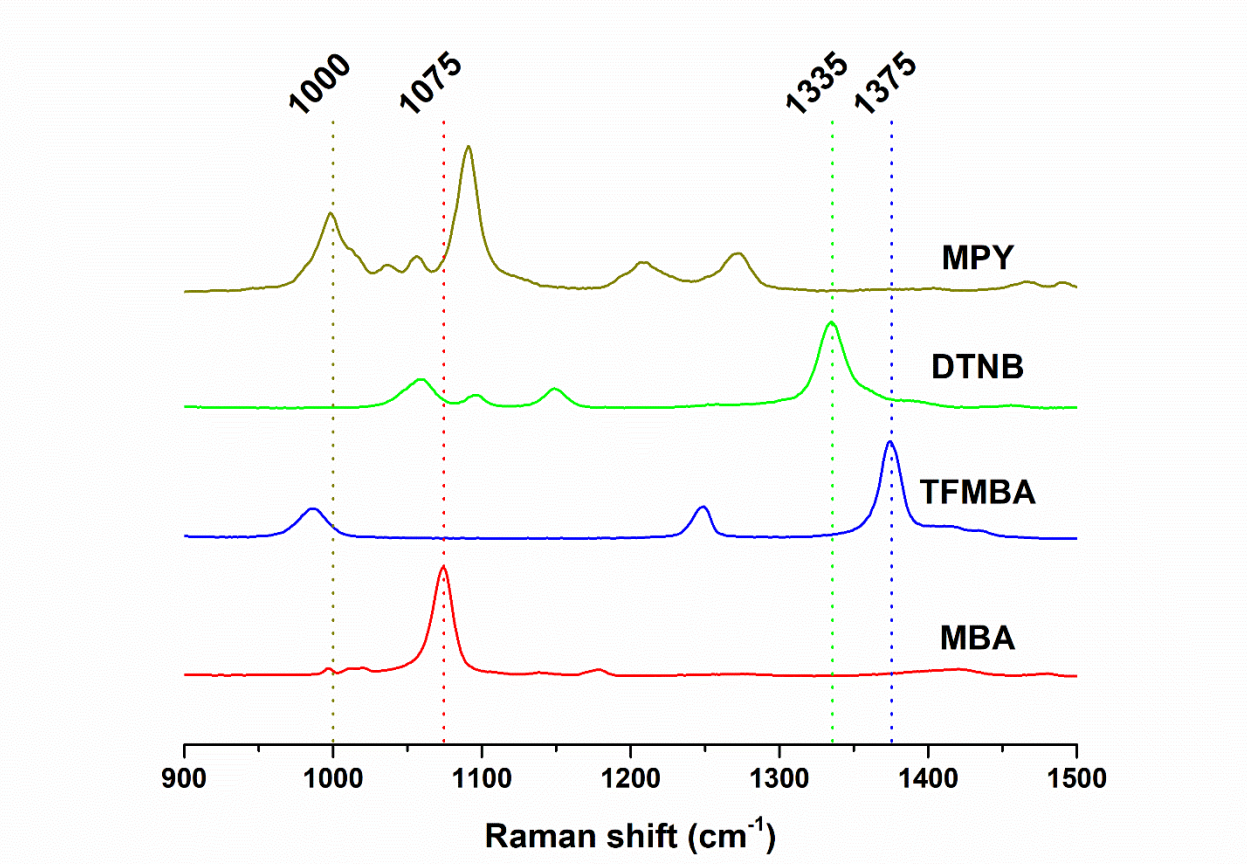

Fig. S2. Raman spectra of SERS barcodes. The SERS barcodes functionalized with MBA, TFMBA, DTNB, and MPY generated unique peaks at 1075, 1375, 1335, and 1000 cm^{-1}, respectively.

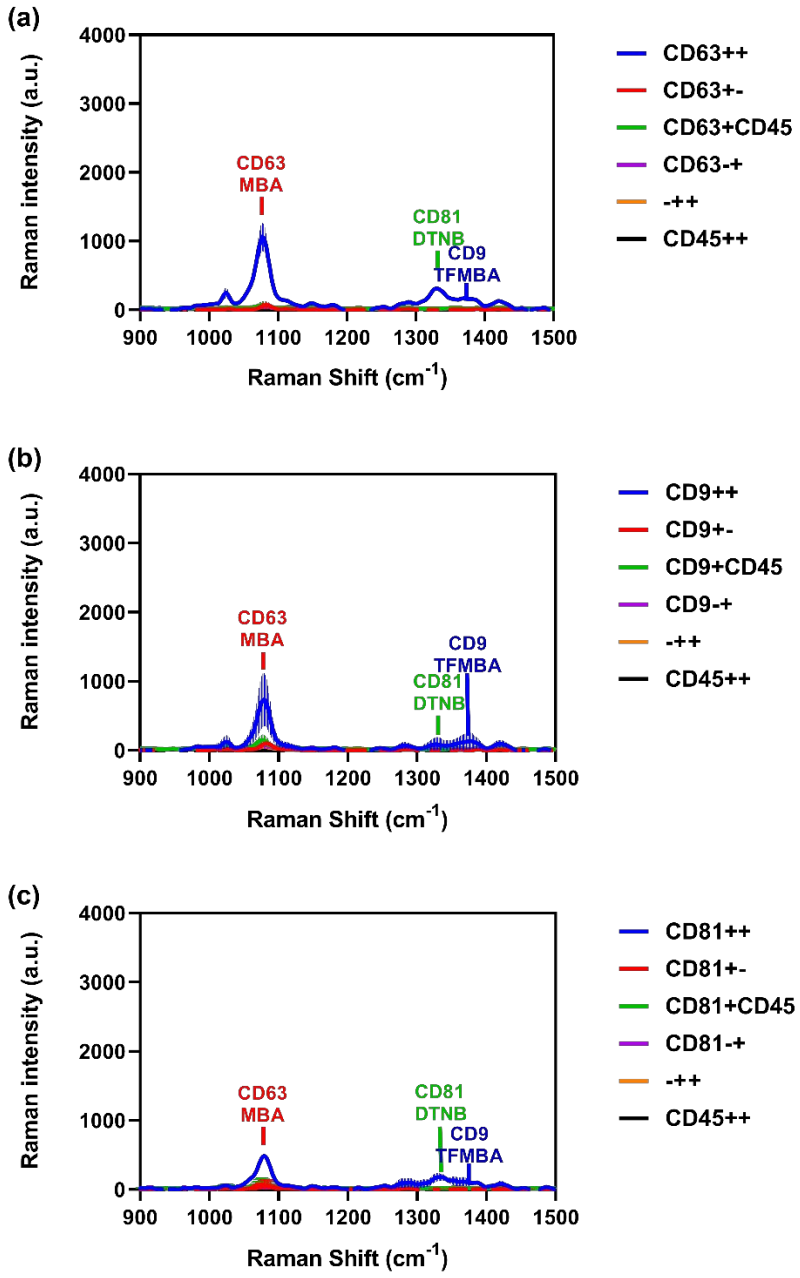

Fig. S3. SERS detection of tetraspanins in SK-MEL-28 cell derived sEVs captured by the (a) anti-CD63, (b) anti-CD9, and (c) anti-CD81 functionalized ESCPs, respectively. Control experiments include without (anti-tetraspanin capture antibody+-) or non-target CD45 detection antibodies (anti-tetraspanin capture antibody+CD45) on SERS barcodes, PBS negative sample controls (anti-tetraspanin capture antibody-+), and without (-++) or non-target CD45 capture antibodies (CD45++) on the surface of sensing units. Data are represented as mean ± s.d., where the shaded area represents s.d. of three separate experiments.

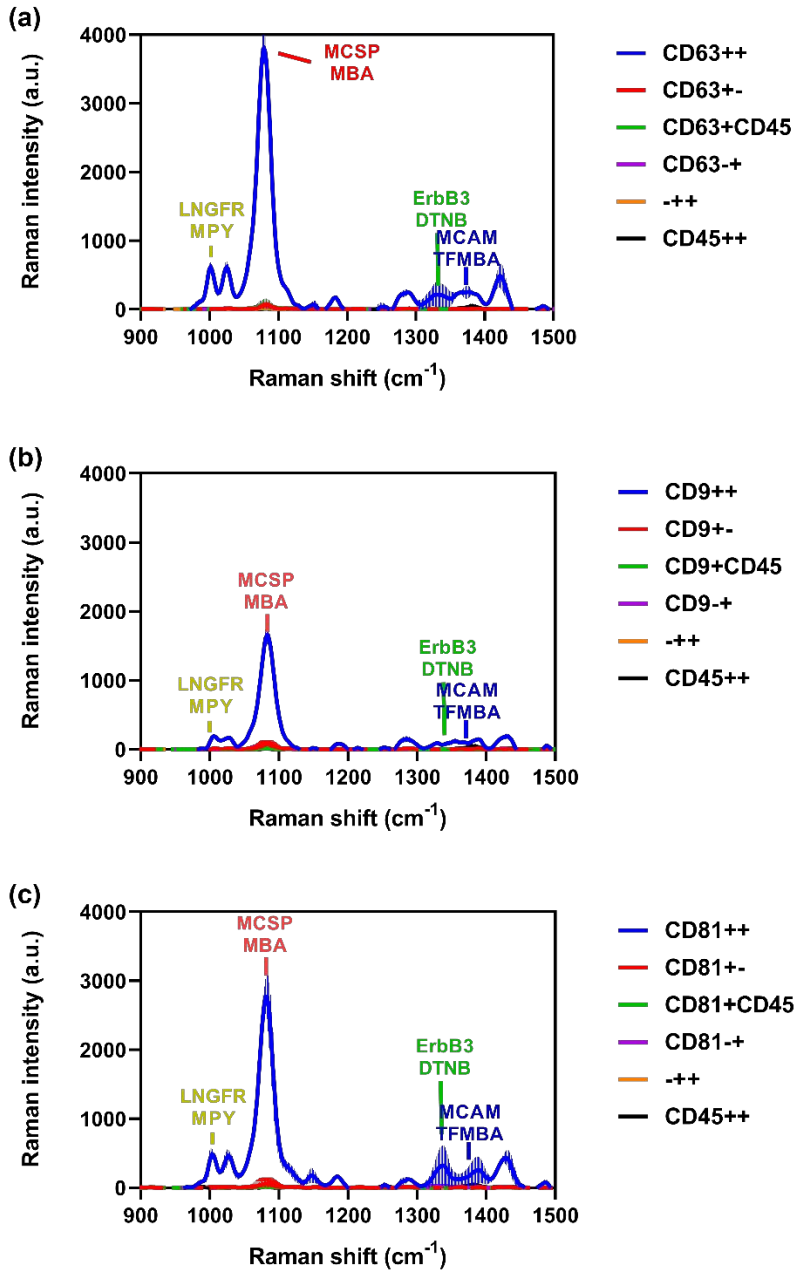

Fig. S4. SERS detection of cancer-associated biomarkers in SK-MEL-28 cell derived sEVs captured by the (a) anti-CD63, (b) anti-CD9, and (c) anti-CD81 functionalized ESCPs, respectively. Control experiments include without (anti-tetraspanin capture antibody+-) or non-target CD45 detection antibodies (anti-tetraspanin capture antibody+CD45) on SERS barcodes, PBS negative sample controls (anti-tetraspanin capture antibody-+), and without (-++) or non-target CD45 capture antibodies (CD45++) on the surface of sensing units. Data are represented as mean ± s.d., where the shaded area represents s.d. of three separate experiments.

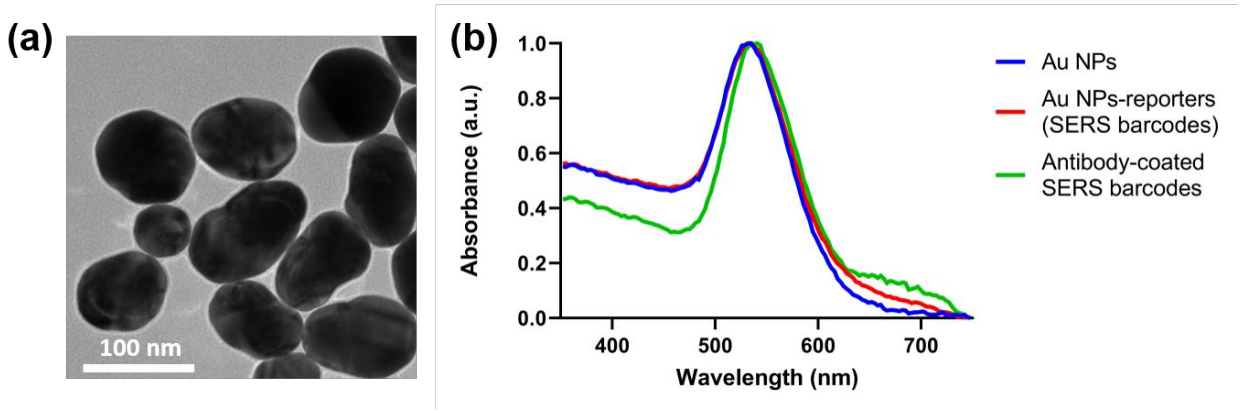

Fig. S5. SERS barcode characterization. (a) A TEM image of gold nanoparticles (Au NPs); (b) UV-vis spectra of Au NPs, Au NPs conjugated with Raman reporters (SERS barcodes), and SERS barcodes functionalized with antibodies.

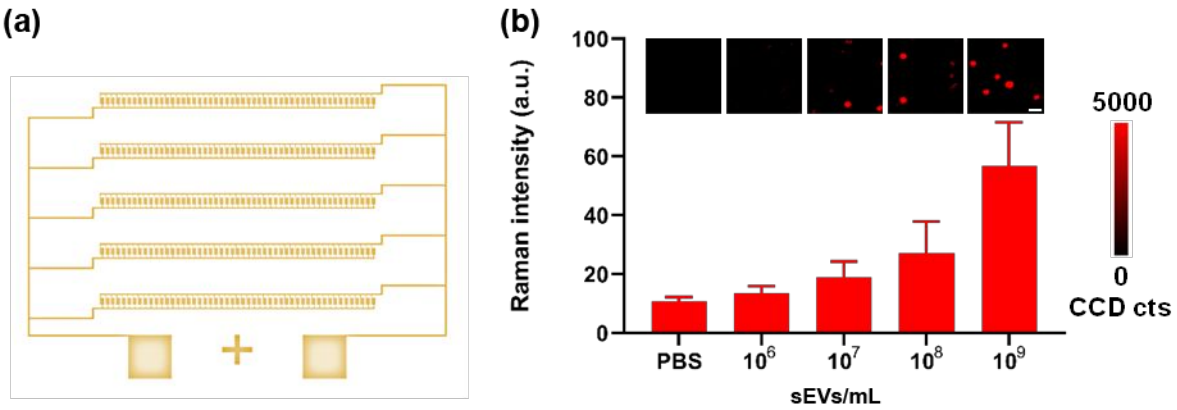

Fig. S6. Sensitivity of the channel microfluidic device. (a) Channel microfluidic device includes five channels, and each channel is made up of an array of 40 pairs of asymmetric gold electrodes. Each asymmetric electrode pair in each channel is connected to individual gold connecting pads that form the cathode and anode. (b) Signal intensities of anti-CD63 SERS barcodes detected from different concentrations of sEVs captured by the anti-CD63 functionalized channel microfluidic device. The insert images are the representative SERS mapping images. Data are represented as mean ± s.d., where error bars represent s.d. of three separate experiments. Scale bar, 10 μm.

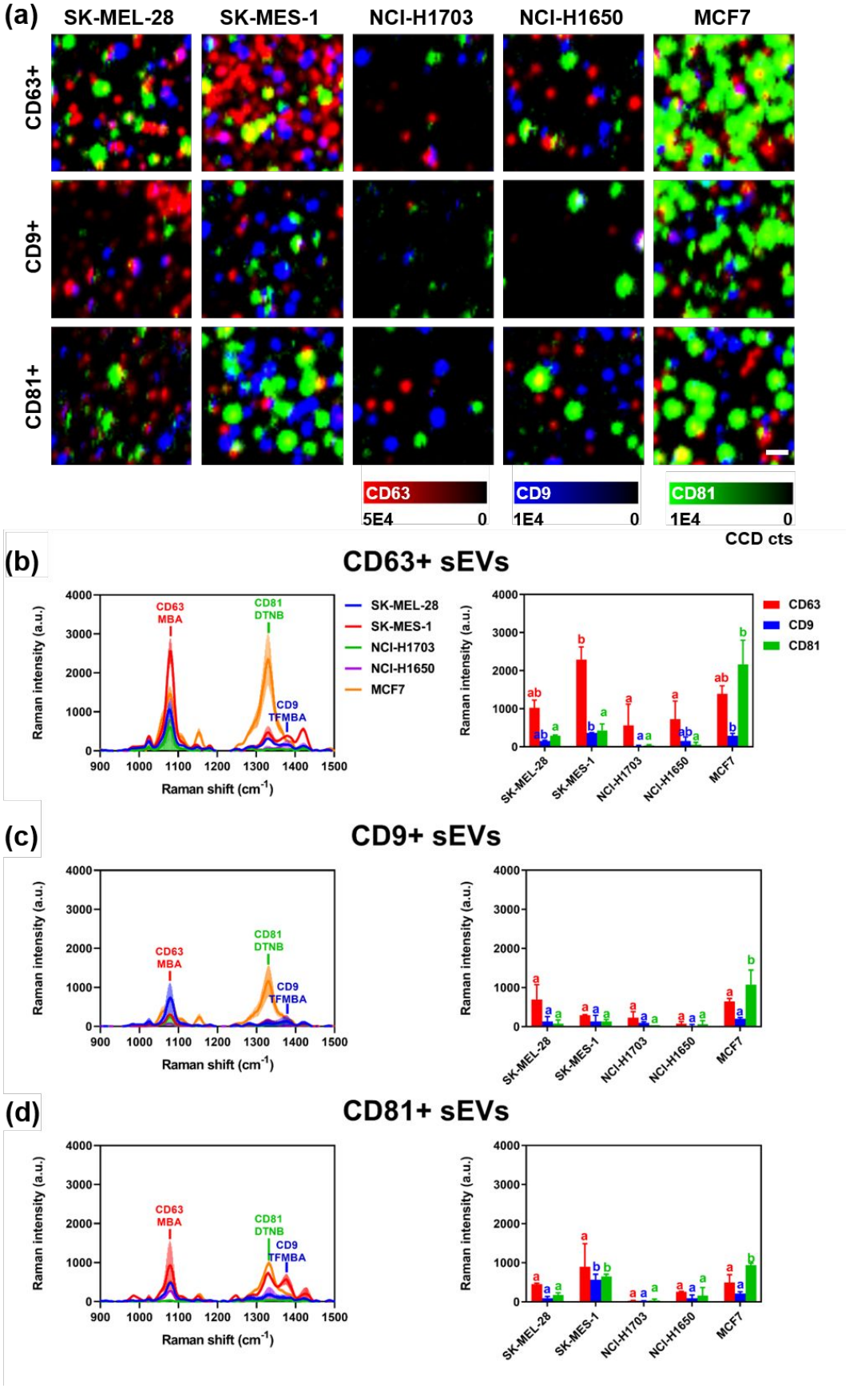
(a)
SK-MEL-28
SK-MES-1
NCI-H1703
NCI-H1650
MCF7
CD63+
CD9+
CD81+
CD63
5E4
0
CD9
1E4
0
CD81
1E4
0
CCD cts
(b)
CD63+ sEVs
Raman intensity (a.u.)
CD63
MBA
CD81
DTNB
CD9
TFMBA
Raman shift (cm-1)
SK-MEL-28
SK-MES-1
NCI-H1703
NCI-H1650
MCF7
CD63
CD9
CD81
(c)
CD9+ sEVs
(d)
CD81+ sEVs

Fig. S7. SERS detection of tetraspanins in different sEV subpopulations derived from cancer cell lines. (a) Representative SERS mapping images, and (b-d) average SERS spectra (left) and characteristic peak intensities (right) detected from sEVs isolated by the anti-CD63, anti-CD9, or anti-CD81 functionalized ESCP, respectively. Red, blue, and green in (a) represent signals generated from anti-CD63, anti-CD9, and anti-CD81 SERS barcodes, respectively. Data in (b-d) are represented as mean ± s.d., where the shaded area and error bars represent s.d. of three separate experiments. Means not sharing a common letter are significantly different ($P < 0.05$). Scale bar, 10 μm.

In Fig. S7a, different colors of signal dots were observed in each SERS mapping image, demonstrating heterogeneous sEV subpopulations. For example, the blue and green colors in the SERS mapping image of SK-MEL-28 cell-derived sEVs captured by the anti-CD63 functionalized ESCP indicated the presence of $CD9^+CD63^+$ and $CD81^+CD63^+$ sEV subpopulations. To statistically compare the sEV phenotypic differences in terms of CD63, CD9, and CD81 biomarkers among selected cancer cell lines, one-way analysis of variance (ANOVA) was applied on the average SERS spectra and characteristic peak intensities (Fig. S7b-d). Capturing by the anti-CD81 functionalized ESCP showed a higher CD9 level in sEVs originating from the SK-MES-1 cell line versus sEVs from other cancer cell lines ($P < 0.05$). Furthermore, CD81 enrichment in MCF7 cell-derived sEVs captured by all anti-CD63, anti-CD9, and anti-CD81 functionalized ESCPs was significantly higher than in other cell lines ($P < 0.05$).

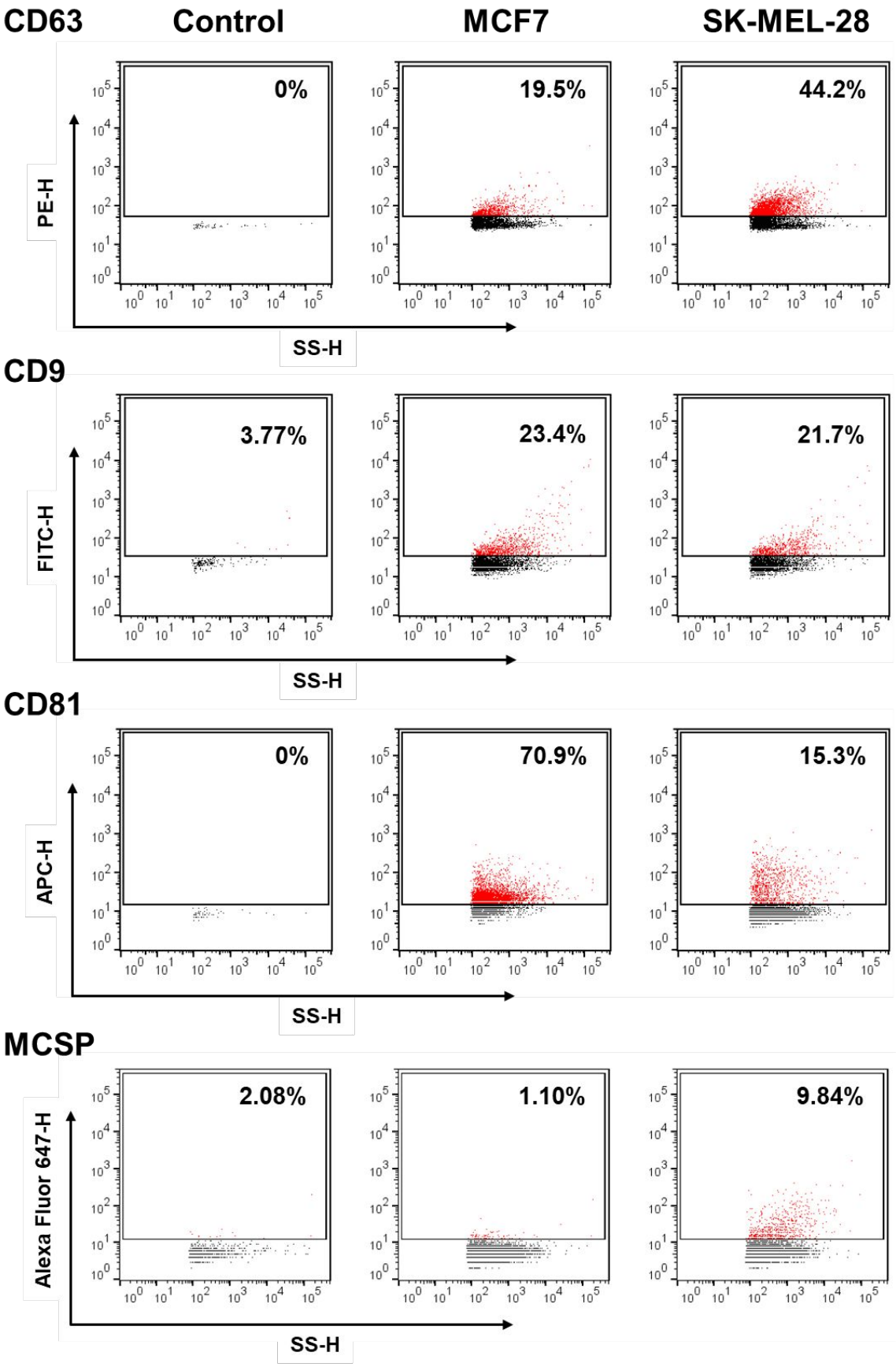
CD63
Control
MCF7
SK-MEL-28
0%
19.5%
44.2%
PE-H
SS-H
CD9
3.77%
23.4%
21.7%
FITC-H
SS-H
CD81
0%
70.9%
15.3%
APC-H
SS-H
MCSP
2.08%
1.10%
9.84%
Alexa Fluor 647-H
SS-H

Fig. S8. Nanoflow cytometry analysis of MCF7 and SK-MEL-28 derived sEVs supports ESCP analysis of tetraspanin proteins and the cancer-associated MCSP. CD9 expression was shown to be relatively consistent between MCF7 and SK-MEL-28-derived sEVs, while $CD63^+$ sEVs were enriched in SK-MEL-28 and $CD81^+$ sEVs were enriched in MCF7. Furthermore, MCSP was shown to be enriched in SK-MEL-28-derived sEVs in comparision to MCF7 sEVs.

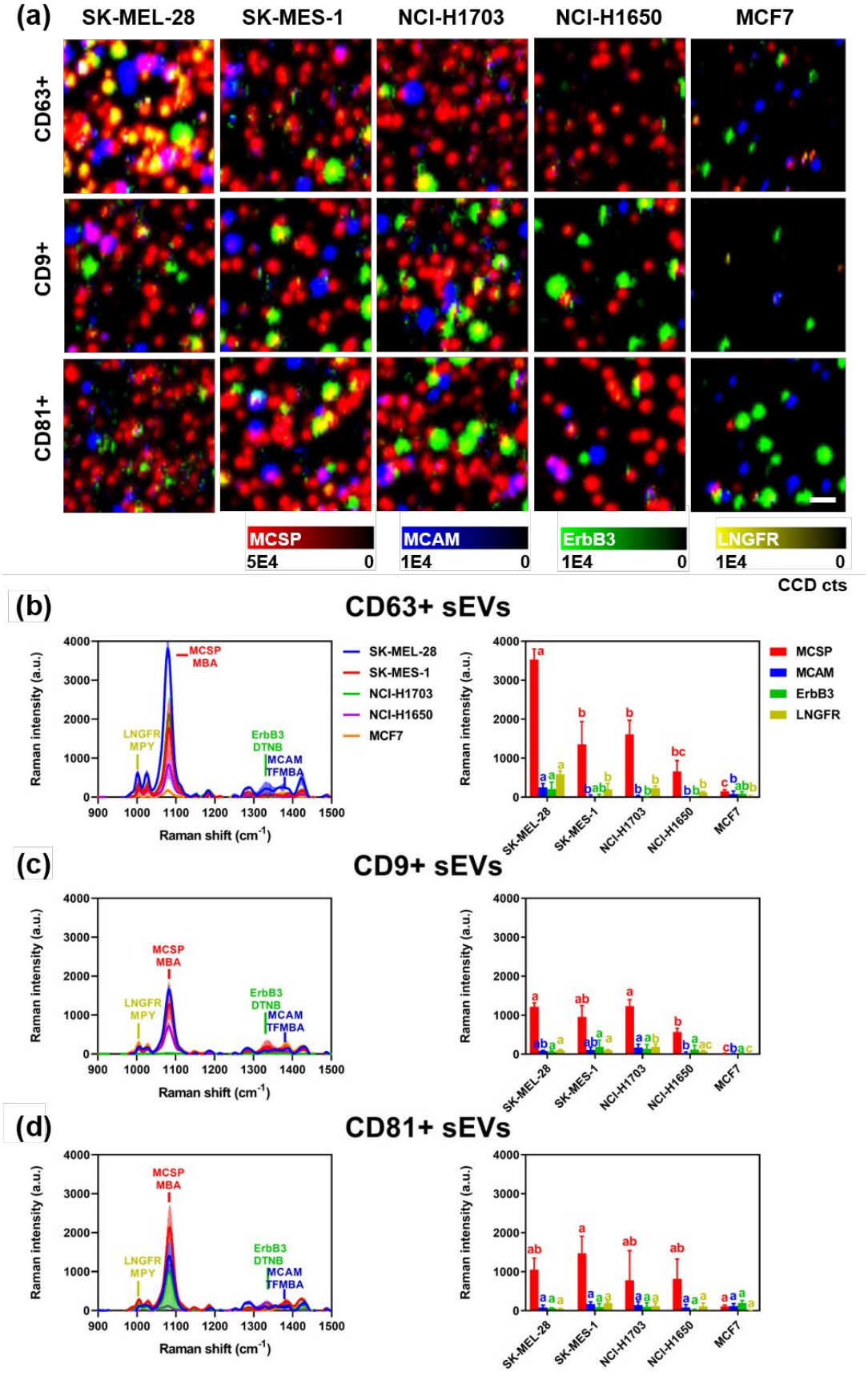
(a)
SK-MEL-28
SK-MES-1
NCI-H1703
NCI-H1650
MCF7
CD63+
CD9+
CD81+
MCSP
5E4
0
MCAM
1E4
0
ErbB3
1E4
0
LNGFR
1E4
0
CCD cts
(b)
CD63+ sEVs
Raman intensity (a.u.)
Raman shift (cm-1)
MCSP
MBA
LNGFR
MPY
ErbB3
DTNB
MCAM
TFMBA
SK-MEL-28
SK-MES-1
NCI-H1703
NCI-H1650
MCF7
(c)
CD9+ sEVs
(d)
CD81+ sEVs

Fig. S9. SERS detection of cancer-associated biomarkers in different sEV subpopulations derived from cancer cell lines. (a) Representative SERS mapping images, and (b-d) average SERS spectra (left) and characteristic peak intensities (right) detected from sEVs isolated by the anti-CD63, anti-CD9, or anti-CD81 functionalized ESCP, respectively. Red, blue, green, and yellow in (a) represent signals generated from anti-MCSP, anti-MCAM, anti-ErbB3, and anti-LNGFR SERS barcodes, respectively. Data in (b-d) are represented as mean ± s.d., where the shaded area and error bars represent s.d. of three separate experiments. Means not sharing a common letter are significantly different ($P < 0.05$). Scale bar, 10 μm.

As shown in Fig. S8a, MCSP was highly abundant in sEVs derived from the selected melanoma and lung cancer cell lines. Further ANOVA analysis on average SERS spectra and characteristic peak intensities (Fig. S8b) indicated that the MCSP level in sEVs captured by the anti-CD63 functionalized ESCP differed significantly among cancer types, following the order melanoma > lung cancer > breast cancer. Notably, MCSP abundance in sEVs captured by either anti-CD9 or anti-CD81 functionalized ESCPs did not exhibit this cell-of-origin dependent trend (Fig. S8c and d). This data explicitly demonstrates that there is inherent inter-sEV heterogeneity and inter-cellular heterogeneity, resulting in cancer-specific biomarkers predominantly being present on particular subpopulations of sEVs.

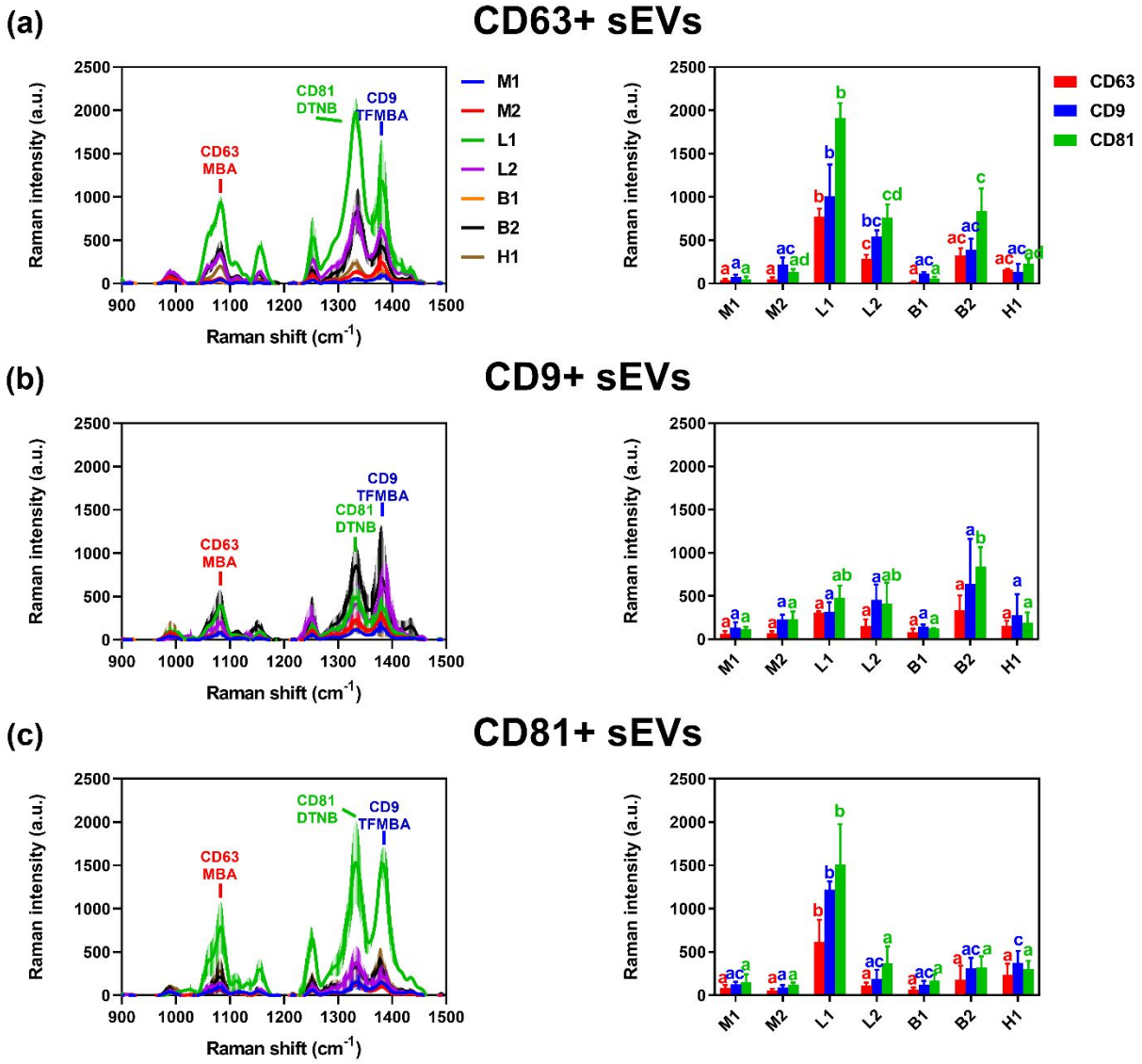

Fig. S10. SERS detection of tetraspanins in plasma sEV subpopulations. Average SERS spectra (left) and characteristic peak intensities (right) in sEVs isolated by the (a) anti-CD63, (b) anti-CD9, or (c) anti-CD81 functionalized ESCP, respectively. Data are represented as mean ± s.d., where the shaded area and error bars represent s.d. of three separate experiments. Means not sharing a common letter are significantly different ($P < 0.05$).

Fig. S9 shows the tetraspanin phenotypes of plasma-sEVs derived from patients and the healthy donor by anti-CD63, anti-CD9, or anti-CD81 functionalized ESCPs, respectively. Plasma derived-sEVs captured by different-antibody-functionalized ESCPs displayed distinct tetraspanin phenotypes. For instance, lung cancer patient 1 had lower expression of target tetraspanins in sEVs

captured by the anti-CD9 functionalized ESCP than anti-CD63 and anti-CD81 functionalized ESCPs, suggesting the inter-sEV heterogeneity in the same patient. We also observed the inter-patient heterogeneity in sEVs. For example, anti-CD63 functionalized ESCP enriched sEVs from lung cancer patients were found to have higher abundance of selected tetraspanin biomarkers compared to other cancer patients' and the healthy donor's (Fig. S9a); tetraspanin phenotypes of anti-CD81 functionalized ESCP enriched sEVs from lung cancer patients 1 and 2 were distinct (Fig. S9c). Taken together, we suggest that it is essential to test the expression of so-called canonical tetraspanin biomarkers in target sEVs and select the target biomarkers according to real applications.

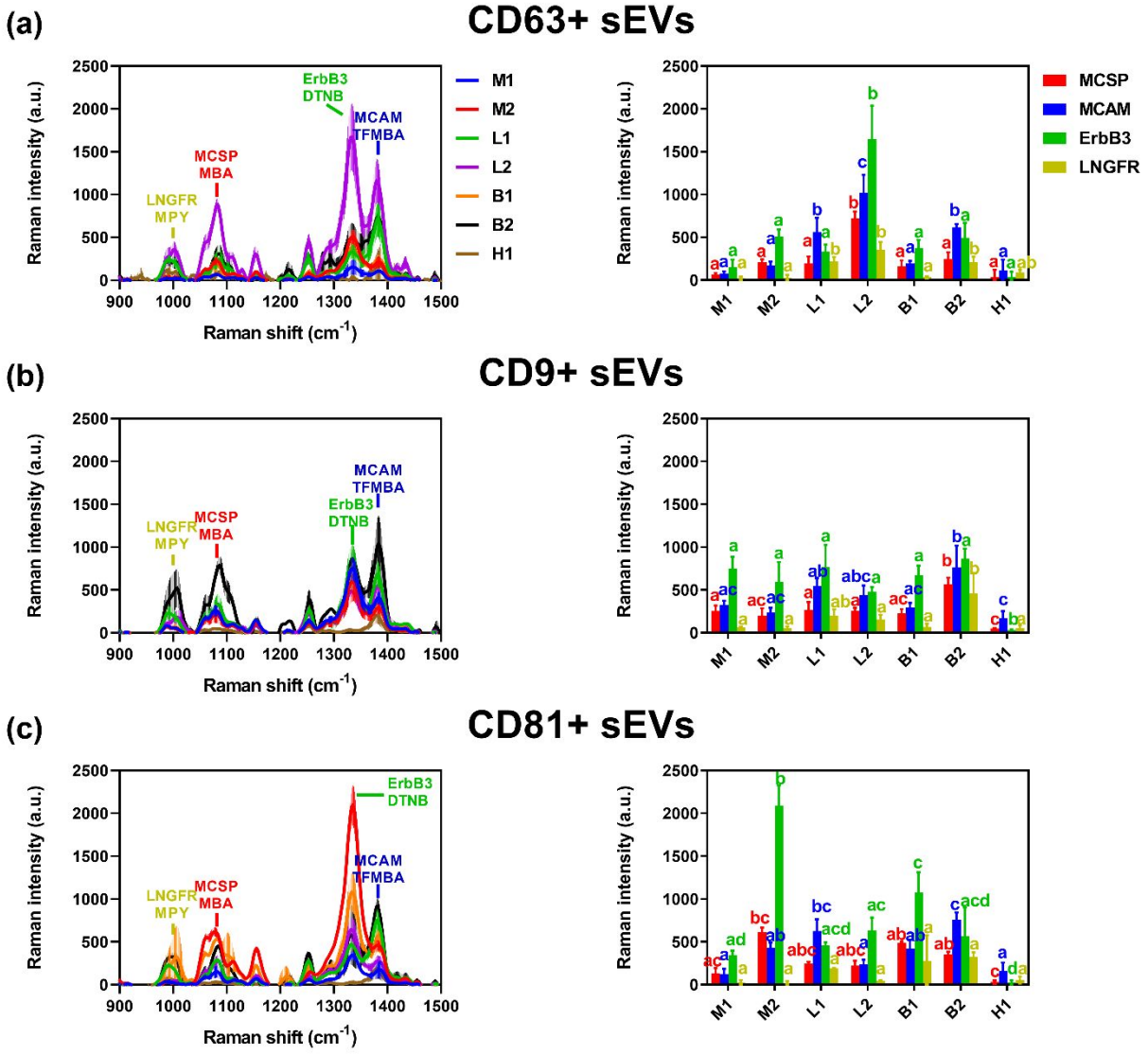

Fig. S11. SERS detection of cancer-associated biomarkers in plasma sEV subpopulations. Average SERS spectra (left) and characteristic peak intensities (right) in sEVs isolated by the (a) anti-CD63, (b) anti-CD9, or (c) anti-CD81 functionalized ESCP, respectively. Data are represented as mean ± s.d., where the shaded area and error bars represent s.d. of three separate experiments. Means not sharing a common letter are significantly different ($P < 0.05$).

The heterogeneity in cancer-associated protein biomarkers was observed among different sEV subpopulations sorted by anti-CD63, anti-CD9, or anti-CD81 functionalized ESCPs (Fig. S10). For lung cancer patient 2, cancer-associated protein biomarkers were shown to be more enriched in sEVs captured by the anti-CD63 functionalized ESCP than anti-CD9 and anti-CD81 functionalized

ESCPs. In addition to the inter-sEV heterogeneity in the same patient is the inter-patient heterogeneity, such as anti-CD63 functionalized ESCP captured sEVs from lung cancer patients 1 and 2 possessing distinct cancer-associated phenotypes (Fig. S10a). These results indicated the selective enrichment of cancer-associated biomarkers in some sEV subpopulations, which might be diagnostically-relevant.

Table S1. Concentrations and median sizes of sEVs measured by the NTA system

Cell lines	Concentrations (particles/ml)	Median (nm)
SK-MEL-28	$1.82\times10^{10} \pm 1.3\times10^{9}$	98.54 ± 2.08
SK-MES-1	$5.26\times10^{11} \pm 3.0\times10^{10}$	99.41 ± 0.34
NCI-H1703	$5.29\times10^{11} \pm 2.1\times10^{10}$	84.48 ± 0.29
NCI-H1650	$1.94\times10^{11} \pm 1.9\times10^{10}$	98.59 ± 0.19
MCF7	$1.10\times10^{10} \pm 5\times10^{7}$	98.87 ± 0.062

Table S2. Demographic information of patients

Patients	**Gender**	**Age**	**Stage**	**Subtype**
M1	M	51.5	IIIB	Superficial spreading melanoma
M2	M	34	IIIB	Nodular melanoma
L1	M	64	IIIB	Adenocarcinoma lung cancer
L2	M	69	IIIB	Adenocarcinoma lung cancer
B1	F	66	IV	HER2-overexpressing breast cancer
B2	F	37	IV	HER2-overexpressing breast cancer